PCCP

The kinetics of the uptake of HNO_3 on ice, solid H_2SO_4–H_2O and solid ternary solutions of H_2SO_4–HNO_3–H_2O in the temperature range 180–211 K†

Arnaud Aguzzi and Michel J. Rossi*

Laboratoire de Pollution Atmosphérique (LPA), Département de Génie Rural (DGR), École Polytechnique Fédérale de Lausanne (EPFL), CH-1015 Lausanne (Switzerland). E-mail: michel.rossi@epfl.ch

Received 15th January 2001, Accepted 22nd June 2001
First published as an Advance Article on the web 7th August 2001

The uptake of nitric acid on ice, solid sulfuric acid solutions and solid ternary solutions was investigated in a Teflon-coated Knudsen flow reactor at 180–211 K using mass spectrometric detection. The uptake coefficient, γ, decreases from 0.30 at 180 K to 0.06 at 211 K. The Arrhenius representation shows two distinct regimes. The first, at low temperatures (180–190 K), shows a constant uptake coefficient, whereas the second, at high temperatures (>195 K), corresponds to an activation energy $E_a = -7 \pm 1$ kcal mol^{-1}. At a fixed temperature the uptake coefficient is independent of the concentration of HNO_3, thus confirming a rate law first order in [HNO_3]. The uptake coefficient of HNO_3 on binary H_2SO_4–H_2O solid solutions decreases linearly from 0.20 at 10 wt.% H_2SO_4 to 0.05 at 98 wt.% H_2SO_4 at 180 K. At 200 K γ decreases from 0.10 to 0.03 over the same concentration range. The uptake coefficient for the heterogeneous interaction of HNO_3 with solid ternary solutions of H_2SO_4–HNO_3–H_2O is 0.10 ± 0.03 in the temperature range 185–195 K under conditions where the composition of the interface was held constant using an external flow of H_2O. HNO_3 uptake on ice fitted a simple Langmuir–Hinshelwood model.

Introduction

Nitric acid plays a key role in atmospheric chemistry in that it is an important trace gas and NO_x reservoir that influences ozone and cloud formation. In particular, the formation of cirrus clouds in the upper troposphere may be promoted by HNO_3 because of its influence on aerosol activation, transforming aerosol particles into cloud condensation nuclei.[1]

Upper tropospheric and lower stratospheric measurements at 54 °N latitude over western Europe yielded HNO_3 mixing ratios between 760 and 1200 ppt.[2] In the lower stratosphere, HNO_3 mixing ratios up to 2500 ppt have been observed over the western/central Pacific at mid-latitudes (37–57 °N) with a mean value of 1510 ppt.[3] Free tropospheric measurements performed by LeBel *et al.*[4] at altitudes below 6 km resulted in an HNO_3 mixing ratio between 20 and 760 ppt over the northeastern Pacific Ocean and between 20 and 560 ppt over the western United States. These results point to the importance of the occurrence of HNO_3 throughout the atmosphere.

In the atmosphere, the main source of HNO_3 is known to be the homogeneous reaction OH + NO_2 + M. However, at high latitudes and in the absence of sunlight, the key reaction for the formation of HNO_3 in the lower stratosphere or upper troposphere is the following heterogeneous hydrolysis proceeding on background H_2SO_4 aerosol particles:[5]

$$N_2O_5(g) + H_2O(s) \rightarrow 2HNO_3(s) \quad (1)$$

Reaction (1) is fast with an uptake coefficient of the order of 0.1 in the temperature range 201–230 K on 60 wt.% H_2SO_4.[6] The destruction of HNO_3 occurs through photodissociation with a yield of approximately 1 from 200 to 315 nm,[7] resulting in OH radical production. Heterogeneous processes of HNO_3 on stratospheric ice particles may result in the formation of polar stratospheric cloud (PSC) type I particles, which are thought to consist of nitric acid trihydrate (NAT), $HNO_3 \cdot 3H_2O$, which is a stable binary form of HNO_3–H_2O under stratospheric conditions.[8]

Other important sources of HNO_3 may be the hydrolysis of $ClONO_2$ and $BrONO_2$ proceeding on sulfuric acid aerosols according to reactions (2) and (3), respectively:

$$ClONO_2(g) + H_2O(s) \rightarrow HOCl(g) + HNO_3(s) \quad (2)$$

$$BrONO_2(g) + H_2O(s) \rightarrow HOBr(g) + HNO_3(s) \quad (3)$$

These reactions have been found to be fast on sulfuric acid[9,10] and on pure ice.[11,12] Reactions (2) and (3) form adsorbed HNO_3, leading to amorphous HNO_3–H_2O mixtures[13] and gaseous HOCl and HOBr, respectively, when taking place on ice or PSC type I particles.[14,15]

The focus of the present work was the kinetic study of the heterogeneous adsorption of HNO_3 on low temperature solid samples, such as pure water ice, H_2SO_4 frozen solutions and solid ternary solutions (STS) of H_2SO_4–HNO_3–H_2O.

The first point to be considered is that we found that pure ice samples may be covered by more than one HNO_3 formal monolayer (ML) before the H_2O vapor pressure starts to decrease, as opposed to the results obtained by Peter *et al.*,[16] who concluded that the rate of evaporation of pure ice begins to decrease when a monolayer of NAT is formed on its surface. This is in agreement with studies performed by Tolbert and Middlebrook,[17] who showed that uncoated ice evaporated faster than ice coated with a formal monolayer of NAT. This is at variance with our results, which show that the rate of evaporation of H_2O over ice starts to decrease after several formal monolayers of HNO_3 have been deposited.

† Electronic Supplementary Information available. See http://www.rsc.org/suppdata/cp/b1/b100546o/

The second aim of this paper is to demonstrate that the use of a Knudsen flow reactor to study HNO_3 uptake on low temperature surfaces leads to results identical with those obtained in laminar flow tube experiments.[18] Moreover, in view of the sometimes conflicting results on the uptake coefficient of HNO_3 on ice, we were able to show that we obtained consistent kinetic results using both steady-state and time-resolved experimental methods. Our methodology rests on a correction scheme which accurately takes into account desorption of HNO_3 from the internal walls of the reaction vessel, a factor which is particularly important in the case of as sticky a molecule as HNO_3. Recent measurements performed by Tolbert and co-workers in a Knudsen reactor resulted only in a lower limit of the uptake of HNO_3 on ice,[13,19] which in fact is lower by a factor of 13 and 450 at 185 and 211 K, respectively, compared with the present results. Nevertheless, their study has the advantage that the condensed phase is probed *in situ* by FTIR absorption concomitantly with the kinetic measurement of HNO_3 uptake on ice.

Experimental

The uptake experiments were performed using an FEP-Teflon-coated Knudsen reactor equipped with a mass spectrometer (MS) as described elsewhere.[20] The characteristic parameters of the reactor are presented in Table 1. The experiments described in this study are based on two different types of protocols: a pulsed-valve (PV) and a steady-state (SS) experiment.

In a PV experiment the gas is introduced into the cell through the pulsed valve at pulse lengths of a few milliseconds. Typical doses range from 10^{13} to 10^{16} molecules per pulse. When the sample chamber is closed the decay of the MS signal of HNO_3 monitored at m/z 46 (NO_2^+) of the so-called reference pulse corresponds to k_{esc}, the escape rate constant for effusion of molecules from the Knudsen flow reactor. The reactive pulse is obtained by admitting an identical pulse with the sample chamber open. The decay of this MS signal, which is the primary observable in a PV experiment, is given by k_{dec} and corresponds to the sum of k_{uni}, the reaction rate constant of interest, and k_{esc} according to the equation

$$k_{dec} = k_{uni} + k_{esc} \quad (4)$$

The PV experiment is a transient supersaturation experiment which permits kinetic studies in real time by measurement of the gas lifetime in the reactor. We also obtain the time dependent rate of formation of the reaction products by monitoring the corresponding MS signal during and just after injection of the reactant. A typical PV experiment is shown in Fig. 1(a).

A typical SS experiment involves introducing a constant flow of gas through a capillary into the Knudsen flow reactor. When a steady state is established, the movable plunger is lifted, so that the reactive condensed phase is exposed to the flowing gas and the rate of uptake may be measured. The change in the MS signal upon opening and closing the sample compartment is related to k_{uni}, which is the primary parameter observable in SS experiments. We assume that the rate law for uptake is first order in the reactant and calculate the value of the rate constant, k_{uni}, according to the equation[20]

$$k_{uni} = k_{sec}\frac{I_0 - I}{I} \quad (5)$$

where I_0 and I are the intensities of the steady-state MS signal levels before and during reaction, respectively. A typical SS experiment is presented in Fig. 2.

The uptake coefficient γ is obtained according to the equation

$$\gamma = \frac{k_{uni}}{\omega} \quad (6)$$

where ω is the collision frequency of the gas with the reactive surface and is calculated from gas kinetic theory (see Table 1)

Table 1 Knudsen cell parameters

Parameter	Value
Volume of the reactor, V	1830 cm^3
Estimated surface area (total)	1300 cm^2
Sample surface area, A_s	17 cm^2
Gas number concentration, [C][a]	(1–1000) × 10^9 cm^{-3}
Surface collision frequency, ω[b]	$\omega = 2A_s(T/M)^{1/2}$ s^{-1}
Escape rate constant, k_{esc}[c]	
For the 8 mm orifice	$0.80(T/M)^{1/2}$ s^{-1}
For the 14 mm orifice	$1.77(T/M)^{1/2}$ s^{-1}

[a] Calculated using the relation $F^i = Vk_{esc}[C]$, where F^i is the flow entering the cell and [C] the concentration. [b] T and M are the temperature and the molecular weight, respectively. [c] Value determined by experiment.

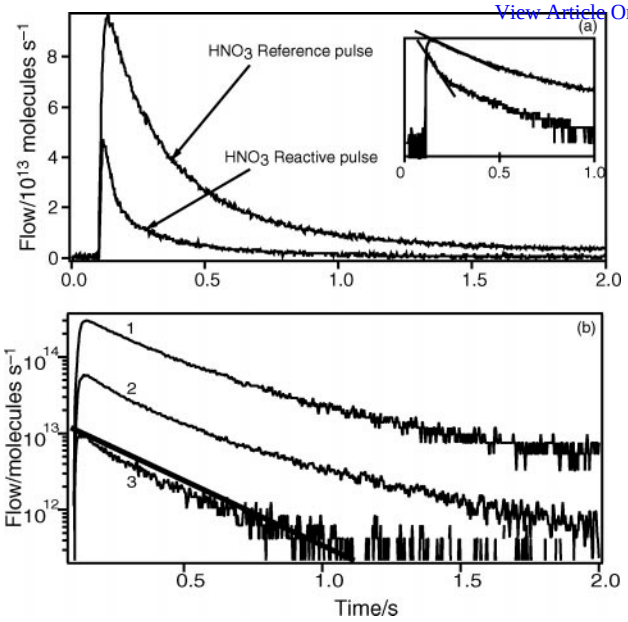

Fig. 1 (a) Typical pulsed valve experiment on HNO_3, monitored at m/z 46, on bulk ice performed in the 14 mm diameter orifice reactor at 180 K using a dose of HNO_3 of 3.5×10^{13} molecules leading to $\gamma = 0.28$. (b) Reference pulses of HNO_3 using doses of (1) 1×10^{14}, (2) 2×10^{13} and (3) 3×10^{12} molecules reveal the complex behavior of HNO_3 on FEP-Teflon. The line represents the decay of a hypothetical non-interacting molecule of mass 63 resulting in $k_{esc} = 3.9$ s^{-1}.

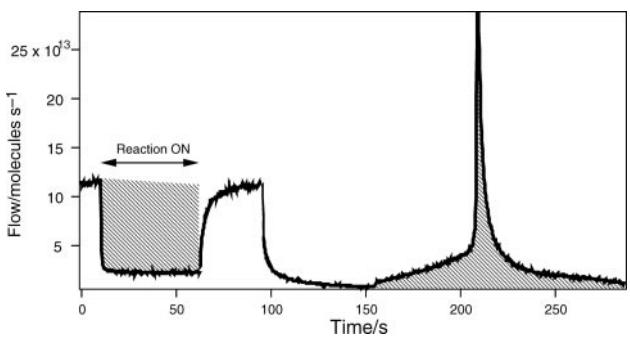

Fig. 2 Typical steady-state experiment on HNO_3 on bulk ice performed in the 14 mm diameter orifice reactor at 200 K at $F^i_{HNO_3} = 1.2 \times 10^{14}$ molecules s^{-1} leading to $\gamma = 0.16$. The first half of the trace represents the uptake of HNO_3 on ice and the second shows the desorption of HNO_3 from the support on warming. Both integrals represented by dashed areas are equal, thus pointing towards a closed mass balance.

to result in $\omega = 74\ s^{-1}$ for HNO_3 at $T = 300$ K taking the geometric surface area of the sample.

The key parameter needed to obtain the uptake coefficient γ is the escape rate constant k_{esc}. Ideally, the value of k_{esc} given by gas kinetic theory depends only on the molecular mass of the gas phase species at a fixed temperature (Table 1). The case of HNO_3 is more complex, as noted by Fenter *et al.*[21] HNO_3 is a sticky compound, the concentration of which on the reactor walls is different for SS and PV experiments owing to differing partial pressures. In PV experiments the MS signal decays faster than expected when calculated by the expression given in Table 1. We therefore obtain an apparent value of the escape rate constant which is larger than the theoretical value. On the other hand, the MS signal decays more slowly in SS experiments when we halt the incoming flow of HNO_3 because of sustained desorption of HNO_3 from the internal walls of the Knudsen reactor. This therefore leads to k_{esc} values that are smaller than expected. The escape rate constant is therefore not the same for both types of experiments, as shown in the Electronic Supplementary Information (ESI).†

The observations in SS and PV experiments are qualitatively understood in terms of HNO_3 adsorption on and desorption from the FEP-Teflon walls of the flow reactor. In PV experiments the walls of the Knudsen reactor act as a sink for HNO_3; before injection of an HNO_3 pulse, the FEP-Teflon coated reactor walls are devoid of HNO_3. When HNO_3 is injected into the reactor on the millisecond time-scale, it will adsorb on the Teflon coating that is applied to the total internal reactor surface and will therefore disappear faster from the gas phase than it would on a non-reactive surface. In SS experiments the internal surfaces of the Knudsen flow reactor are covered with adsorbed HNO_3, the coverage of which depends on the flow rate of HNO_3 into the reactor, and hence on the partial pressure of HNO_3, P_{HNO_3}. In order to determine k_{esc}, the flow of HNO_3 is halted and the resulting decay of P_{HNO_3}, the rate of change of which directly leads to k_{esc}, is monitored. However, during the decrease of P_{HNO_3} owing to the interaction of HNO_3 with the condensed phase, adsorbed HNO_3 desorbs from the Teflon-coated internal surfaces, which act like a reservoir for HNO_3 and therefore give rise to an HNO_3 source term. The net result is a decrease in k_{esc} owing to the replenishment of gas phase HNO_3 (P_{HNO_3}) with formerly adsorbed HNO_3, thus leading to an effect in k_{esc} opposite to that observed in PV experiments. Using the 14 mm escape orifice reactor, we calculate a value of k_{esc} of 3.9 s^{-1} for HNO_3 according to gas kinetic theory, whereas PV experiments give k_{esc} of $(5 \pm 1)\ s^{-1}$ and SS experiments result in $k_{esc} = 2 \pm 1\ s^{-1}$. In all experiments we measured k_{esc} for the specific experimental conditions before each uptake experiment and used this value to determine γ according to eqns. (4)–(6).

Regarding PV experiments, a simple model was developed by Fenter *et al.*[21] to separate wall contributions from escape. The decrease of both reference and reactive MS signals can be approximated by a double exponential decay. The inset in Fig. 1(a) shows the decay of both pulses. The effects of the internal reactor surfaces for a PV experiment are present to approximately the same extent in both pulses and therefore almost cancel. Although the HNO_3–FEP-Teflon interaction was not studied quantitatively in this work, we would stress that the present measurement is a difference measurement of the initial slopes as shown in the inset in Fig. 1(a), whereby the complex decay pertaining to the reference pulse cancels to a large extent.

A detailed discussion of the chemical–kinetic mechanism of the interaction of HNO_3 with the FEP-coated internal walls of the Knudsen flow reactor is clearly outside the scope of this work. However, Fig. 1(b), which displays the decay of the MS signal of HNO_3 as a function of time at three different doses, underlines the strong sensitivity of the decay rate and thus the gas lifetime of HNO_3 on the dose or its initial transient partial pressure. Three qualitative observations may be made based on inspection of the three reference experiments presented in Fig. 1(b):

1. The initial slope of MS signals 3 and 2 is larger than the reference representing a non-interacting molecule of mass 63. The slope of signal 1 pertaining to a dose larger by a factor of approximately 30 compared with signal 3 is equal to the theoretical reference of $k_{esc} = 3.9\ s^{-1}$. This is consistent with increasing HNO_3 desorption from the wall even during the decay with increasing HNO_3 dose.

2. At a low dose (signal 3), there is no lingering "memory" effect of desorbing HNO_3 as the MS signal fairly rapidly goes to zero. At a high dose such as for signal 1 so much HNO_3 has adsorbed on the Teflon walls that they become a (pseudo-) steady-state source of HNO_3 after approximately 2 s at a level of 2.3% of the initial amplitude of the MS signal. This then means that the walls act as a steady-state reservoir for HNO_3 at high dose akin to high continuous flow rates.

3. The mechanism of the HNO_3 interaction with the FEP-coated internal walls of the Knudsen flow reactor is complex, that is non-exponential, and perhaps merits a study in its own right.

In contrast to PV experiments, a correction to the measured value of γ_{obs} has to be applied in SS experiments. Fig. 3 shows a typical SS experiment where I_0 and I are the observed MS intensities obtained during an uptake experiment. In an SS experiment there is a steady state between HNO_3 adsorption and desorption processes on the internal surfaces of the Knudsen flow reactor before opening the sample chamber as well as during the uptake experiment. When the condensed phase is exposed to the gas phase at $t = 15$ s, a fast partial pressure drop of HNO_3 occurs, because the ice substrate acts as a cryogenic pump. Owing to the decrease in the HNO_3 partial pressure, the steady state between the rate of HNO_3 adsorption and desorption on the walls is perturbed. A significant amount of HNO_3 molecules desorbs from the walls during the reaction, thus increasing the MS signal at m/z 46 so that the level observed during the reaction is higher than it would be in the ideal case of a non-sticky molecule.

To correct the experimental γ_{obs} value, one makes the following assumptions. First, the hatched area displayed in Fig. 3 resulting from the sluggish recovery of the initial MS signal level of HNO_3 on closing the sample compartment corresponds to the number of molecules, N, which desorb from the walls during the reaction. If no HNO_3 stuck to the walls during a SS experiment, the HNO_3 MS signal would rise instantaneously on the chosen time-scale at the end of the uptake experiment, and would therefore not be delayed as observed in Figs. 2 and 3. The second assumption is that this additional source of HNO_3 appearing during reaction con-

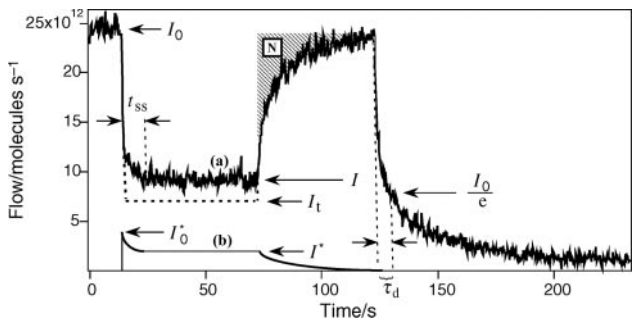

Fig. 3 Bold trace (a) shows an experimental MS signal of HNO_3 at m/z 46 observed at 210 K; the dashed line represents the expected signal if there were no wall contribution during the uptake experiment. The bold trace (b) is the calculated additional source of HNO_3 in order to correct the value of the HNO_3 uptake coefficient (see text for details).

tributes to a partial, albeit hypothetical, flow rate I_0^* given by $I_0^* = N/t_{ss}$ molecules s^{-1}, where t_{ss} is the time necessary to reach steady state during the uptake. When the HNO_3 flow rate is halted at $t = 125$ s, one may determine the rate constant for HNO_3 desorption from the internal walls, $k_d = 1/\tau_d$, by measuring the time, τ_d, necessary to observe the decay of the MS signal to I_0/e (see Fig. 3). All τ_d values are in the range 10–20 s, which results in the desorption kinetics of HNO_3 from the walls falling in the range between 0.05 and 0.10 s^{-1}. The measured values of t_{ss} measured upon HNO_3 uptake seem to be a multiple of τ_d measured at the end of the uptake experiment (Fig. 3).

Fig. 3 displays an experimental trace obtained at a substrate temperature of 210 K (trace a). We make the assumption that the dashed line just below trace a would be the true (calculated) SS signal level if there were no contribution from HNO_3 desorbing from the internal surfaces. The reactor walls are considered as a constant source of HNO_3 during the uptake experiment because of the large reservoir of HNO_3 extending over 1300 cm^2 of the internal reactor area. In this case, one may express the true uptake coefficient γ_t by eqn. (7) if I_t were known. Trace b in Fig. 3 shows the calculated additional HNO_3 flow rate I^* at the steady state due to the desorption of N molecules of HNO_3 from the walls. Before opening the sample compartment, there is no additional flow as there is a steady state between the rate of adsorption and desorption of HNO_3. On opening the sample chamber at $t = 15$ s, the N molecules of HNO_3 desorb from the walls and react on the ice sample according to γ_t, which may be expressed by eqn. (8).

$$\gamma_t = \frac{k_{esc}}{\omega}\left(\frac{I_0}{I_t} - 1\right) \quad (7)$$

$$\gamma_t = \frac{k_{esc}}{\omega}\left(\frac{I_0^*}{I^*} - 1\right) \quad (8)$$

Eqn. (7) gives the true uptake coefficient γ_t for the external source, while eqn. (8) results in the identical value for γ_t owing to HNO_3 desorbing fom the walls (internal source). This equation system is made up of two equations with three unknowns, γ_t, I^* and I_t, and three known parameters, I_0, I (measured) and I_0^* (calculated, see above). Both equations have been set equal to each other, and by making the assumption that $I^* = I - I_t$, the resolution of this system leads to the following expression for γ_t:

$$\gamma_t = \gamma_{obs} + \frac{k_{esc} N}{\omega t_{ss} I} \quad (9)$$

where $\gamma_{obs} = (k_{esc}/\omega)[(I_0/I) - 1]$ is the experimental value for the uptake obtained using the measured initial and final MS signal intensities I_0 and I in eqns. (5) and (6), k_{esc} is the escape rate constant, N the total number of HNO_3 molecules desorbing from the walls, ω the collision frequency with the reactive surface and t_{ss} the time necessary to reach steady state after lifting up the plunger: t_{ss} is of the same order as the decay time of the MS signal once the HNO_3 flow rate has been halted.

The procedures to obtain different ice samples are the following. "Bulk ice" (B) was obtained by pouring liquid deionized water into the sample dish prior to any experiment. The water was then degassed by freeze–pump–thaw cycles and finally cooled to a chosen temperature in order to perform the uptake experiment.

"Condensed ice" (C) was obtained by depositing water vapor on the cold support at 150 K. The empty support was attached to the reactor and subsequently cooled to the desired temperature with the plunger lowered, that is, the sample compartment sealed off. When the chosen temperature had been reached (150 K), the plunger was lifted and the sample dish was exposed to a high water flow of the order of 10^{19} molecules s^{-1} for several minutes. This resulted in an average sample size of about 10^5 formal monolayers (ML) of 250 nm total thickness.

The frozen H_2SO_4 samples were prepared in two steps. First, a bulk ice sample was prepared at 150 K by freezing a small amount of liquid H_2O in order to protect the gold-plated sample support from the corrosive action of H_2SO_4. Subsequently, a liquid H_2SO_4 solution was slowly added to the bulk ice layer, which froze immediately so as to avoid any concentration gradient or dilution in the bulk. The thicknesses of the two layers were generally similar, typically 0.5 cm. Solid ternary solution (STS) samples consisting of H_2SO_4–HNO_3–H_2O were prepared in the same manner as the frozen H_2SO_4–H_2O samples.

Gas phase HNO_3 was prepared from a mixture of liquid HNO_3 (90%, Fluka) stabilized in H_2SO_4 (98%, Fluka) in a ratio of 1 : 3 v/v.

Results and discussion

A. HNO_3 on ice

1. Kinetic results. We performed steady-state (SS) and pulsed-valve (PV) experiments on two different types of ice, namely bulk ice (B) and condensed ice (C) at temperatures from 180 to 211 K. Typical uptake experiments of nitric acid on ice are shown in Fig. 1(a) and 2. Most of the experiments were carried out using the 14 diameter orifice reactor (see Table 1).

Fig. 1(a) shows a PV experiment performed at 180 K. The large pulse is the reference pulse whose decay is given by $k_{esc} = 4.3$ s^{-1}. The small pulse is the reactive one, with the sample chamber open, resulting in $k_{dec} = 23.9$ s^{-1}, corresponding to an uptake coefficient of 0.28 ± 0.08, where uncertainties are determined by the MS signal noise. The inset in Fig. 1(a) shows a semilogarithmic plot of both the reference and the reactive pulse. Deviations from first order decay kinetics are apparent for both pulses at late times, in keeping with the complications discussed above. Fig. 2 shows an SS experiment performed at 200 K. When the ice sample is exposed to HNO_3 a rapid drop of the MS signal at m/z 46 is observed and a steady-state level is reached after a few seconds (t_{ss}) corresponding to $\gamma = 0.16 \pm 0.05$ at 200 K. When the sample chamber is closed at $t = 60$ s in order to stop the uptake, we observe that the MS signal increases only slowly to reach its initial level, which we attribute to adsorption of HNO_3 on the reactor walls as discussed above. Subsequently, the flow rate of HNO_3 entering the reactor is halted and the temperature of the support is increased at $t = 155$ s with the movable plunger open in order to let HNO_3 evaporate from the previously exposed ice substrate. The evaporation rate is at a maximum at $t = 215$ s and corresponds to the peak signal displayed in Fig. 2 which appears at 218 ± 3 K using the 14 mm escape reactor orifice. In all uptake experiments the number of HNO_3 molecules condensing on both types of ice (B and C) is equal to the number desorbing from the condensed phase on increasing the temperature, thus resulting in a closed mass balance in the uptake experiments such as those shown in Fig. 2.

The results on the uptake kinetics of HNO_3 on ice are displayed in the ESI† for the temperature range 180–211 K. We note the discrepancy of k_{esc} determined in PV and SS experiments, which was assigned to the contribution of the reactor walls. In PV experiments, k_{esc} is increased owing to HNO_3 loss on the reactor walls, whereas in SS experiments, k_{esc} is smaller owing to HNO_3 desorption from the walls, as discussed above. In PV experiments, k_{esc} is twice as large as in SS experiments. At a specific temperature, the uptake coefficients

γ_{obs} obtained in PV and SS experiments are independent of the dose and the flow entering the reactor, respectively, and therefore of the concentration of HNO_3. This confirms a first order rate law for the uptake process whose rate constant k_{uni} was obtained from eqn. (4) for PV experiments and from eqn. (5) for SS experiments. Although the observed γ values obtained in SS experiments are in general 15% smaller than those obtained in PV experiments, they are indistinguishable, as shown in the Arrhenius representation displayed in Fig. 4 once the correction according to eqn. (9) has been applied to the SS experiments. Not all γ values were corrected, owing to experimental problems. At 180, 190, 200 and 210 K, the γ values displayed in Fig. 4 have been shifted for clarity by +0.5 and −0.5 K for SS and PV experiments, respectively, in keeping with uncertainties of the temperature measurement.

Fig. 4 clearly shows two distinct regimes of temperature dependence. In the high temperature regime, k_{uni} or γ changes faster with temperature compared with the low temperature regime. The uptake coefficient γ drops from 0.30 at 180 K to 0.06 at 211 K and therefore corresponds to a negative temperature dependence. At these relatively high temperatures, the low values of γ may be attributed to a significant evaporation rate, resulting in a significant decrease of the net HNO_3 uptake, of the order of a factor of 5, akin to the uptake coefficient of $D_2{}^{18}O$ on $D_2{}^{16}O$ ice samples.[22] The transition temperature between these two regimes is approximately 195 ± 5 K, similar to the transition temperature for $D_2{}^{18}O$ observed by Chaix *et al.*[22] At $T < 195$ K, we did not observe any temperature dependence of γ, which was constant at 0.26 ± 0.09. From the temperature dependence of k_{uni} observed at $T > 195$ K, we determined an activation energy $E_a = -6.8 \pm 1.0$ kcal mol^{-1} for the adsorption process of HNO_3 on both types of ice. Despite the simple first order rate law for HNO_3 adsorption on pure ice, the negative temperature dependence of k_{uni} and γ leads to a complex adsorption mechanism. In Section D we present modeling results of our experimental kinetic data according to a Langmuir–Hinshelwood mechanism involving a precursor to HNO_3 adsorption.

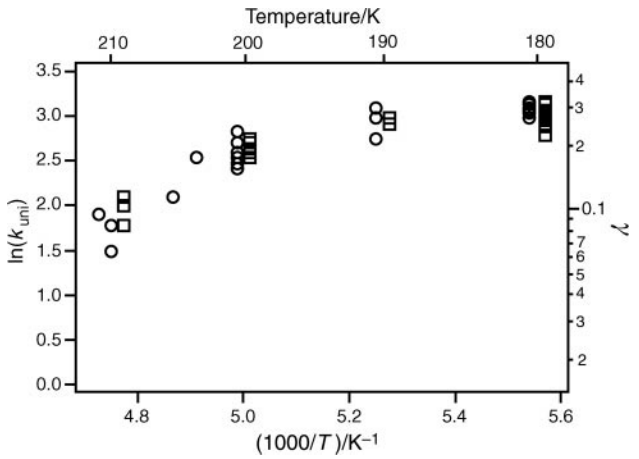

Fig. 4 Arrhenius representation of the uptake rate constant of HNO_3 on bulk ice and condensed ice (confounded), obtained in pulsed valve (squares) and steady-state (circles) experiments, the latter of which were corrected using eqn. (9).

Table 2 summarizes the kinetic results obtained in this study and previous results obtained in other laboratories.[13,18,19,23–25] The uptake coefficients γ_0 for HNO_3 on ice samples reported here (see the ESI†) are in good agreement with the lower limits reported by Hanson[18] at 191 and 200 K. As shown in Table 2, most workers using the flow tube technique gave only lower limits for the uptake coefficient of HNO_3 on ice owing to the large value of γ. Abbatt[24] obtained a γ value higher than 0.2 at 218 K, which appears to be too large at this temperature compared with our result at 210 K. Owing to rate-limiting gas phase diffusion of HNO_3, flow tube experiments can give only limited information in the case of rapid kinetics such as in the present case. Tolbert and co-workers[13,19] gave lower limits for the initial uptake coefficient γ_0 obtained in their Knudsen reactor, and γ_{ss} is significantly smaller when steady state is reached, amounting to a factor of 300. At 211 K, we observe partial saturation of the ice sample as was also observed by Tolbert and co-workers. The low γ values found by Tolbert and co-workers[13,19] may perhaps be explained by wall contributions during HNO_3 uptake. Their experimental apparatus has a large ratio of internal to reactive surface area, which may possibly lead to significant quantities of HNO_3 desorbing from the reactor walls. This in turn would lead to higher than expected values of the partial pressure of HNO_3 under steady-state conditions, resulting in a small net HNO_3 uptake on the ice and thus to low γ values.

2. Condensed phase product. The investigations of the uptake of HNO_3 on ice samples for a temperature range of 180–200 K show a constant uptake over the time-scale of 50 s (Fig. 2). We performed prolonged uptake experiments of HNO_3 interacting with the condensed ice (C) substrate in order to determine the mean stochiometric ratio between H_2O and HNO_3 in the condensed phase. This type of experiment allowed us to determine the average concentration of the condensed substrate from mass balance arguments at certain selected discontinuities of the HNO_3 partial pressure curve with time. It was performed on condensed ice whose thickness and temperature are shown in the ESI† in addition to the results obtained for n, which is the ratio of H_2O remaining in the condensed phase to HNO_3 condensed on the ice sample when abrupt changes in P_{HNO_3} appear at $t = 210$ and 550 s, as displayed in Fig. 5(a) and (b), respectively. Raw data are displayed in Fig. 5, where panels (a) and (b) show experiments performed on condensed ice samples at 180 and 200 K,

Table 2 Uptake coefficients, γ, of HNO_3 on ice

T/K	γ	Experimental technique/detection[a]	Ref.
185	>0.02	Knudsen reactor/MS, FTIR-RAS	Zondlo *et al.*, 1998[13]
191	⩾0.30	Flow tube/CIMS	Hanson, 1992[18]
197	$0.3^{+0.7}_{-0.1}$	Flow tube/MS	Leu, 1988[23]
200	⩾0.20	Flow tube/CIMS	Hanson, 1992[18]
200	0.30	Knudsen reactor/MS	Seisel *et al.*, 1998[25]
211	$\gamma_0 \geqslant 0.005$	Knudsen reactor/MS, FTIR-RAS	Zondlo *et al.*, 1997[19]
	$\gamma_{ss} = 0.0002$	Knudsen reactor/MS, FTIR-RAS	Zondlo *et al.*, 1997[19]
218	>0.20	Flow tube/MS	Abbatt, 1997[24]
180	0.27 ± 0.08	Knudsen reactor/MS	This work
190	0.25 ± 0.10	Knudsen reactor/MS	This work
200	0.17 ± 0.05	Knudsen reactor/MS	This work
210	0.09 ± 0.03	Knudsen reactor/MS	This work

[a] CIMS = chemical ionization mass spectrometry; MS = mass spectrometry; FTIR-RAS = Fourier transform infrared reflection–absorption spectroscopy.

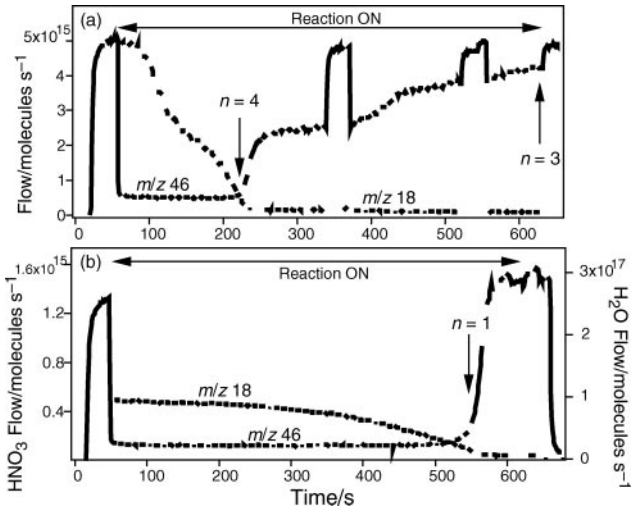

Fig. 5 Steady-state uptake experiments on HNO_3 (m/z 46) on condensed ice on a long-time scale at (a) 180 K using the 14 mm orifice reactor and (b) 200 K using the 8 mm orifice reactor. H_2O was monitored at m/z 18. The mean concentration ratio HNO_3 : H_2O of the condensed mixture is expressed as n.

respectively. We recorded both HNO_3 (m/z 46) and H_2O (m/z 18) in order to obtain an accurate mass balance for both components at any given point in time. Abrupt changes of the partial pressure of HNO_3 were observed at m/z 46 at $t = 550$ s [Fig. 5(b)] and $t = 210/640$ s [Fig. 5(a)] at 200 and 180 K, respectively.

The abrupt change of the HNO_3 partial pressure is assumed to be a change in the phase of the sample (phase transition). Concurrently, we measured the number of H_2O molecules that desorbed from the ice sample by monitoring the partial pressure of H_2O at m/z 18. When we compare the number of H_2O molecules making up the sample prior to the uptake experiment and the number of H_2O molecules which have desorbed at a given time, one is able to determine the amount of ice remaining on the support at any given time. For instance, in the case displayed in Fig. 5(b) we condensed 2.87×10^{19} H_2O molecules, resulting in an ice sample of approximately 670 nm. During the HNO_3 uptake experiment, 2.82×10^{19} H_2O molecules desorbed from the sample surface. Therefore, 5.3×10^{17} H_2O molecules still remain on the support at 550 s. At the same time, 5.9×10^{17} HNO_3 molecules have been adsorbed on the ice sample, leading to a mean stochiometric ratio between H_2O and HNO_3 in the condensed phase of $n = 0.9$ (see ESI†). The ice surface was not equilibrated by an external H_2O flow, in order to be able to follow the change in the H_2O MS signal at m/z 18.

At 180 K, we observe two distinct levels of HNO_3 during the uptake [Fig. 5(a)] in contrast to experiments performed at 200 K [Fig. 5(b)] and 190 K (not shown). At 200 K [Fig. 5(b)], we calculate a mean composition of the solid substrate of $HNO_3 \cdot 1H_2O$ at $t = 550$ s. The ratio calculated at 180 K and $t = 210$ s shows a mean composition of the solid substrate of $HNO_3 \cdot 4H_2O$ when the net uptake of HNO_3 begins to decrease. At the end of the uptake at $t = 640$ s we found a mean composition of $HNO_3 \cdot 3H_2O$ [see Fig. 5(a)]. At this temperature, which is below the ice frost point, we apparently obtain a mean stoichiometry corresponding to NAT across the average of the condensed phase, namely HNO_3 : H_2O = 1 : 3 when it is exposed for a long time to gaseous HNO_3. In contrast, at 190 and 200 K one obtains an average condensed phase having a mean stoichiometry of HNO_3 : H_2O = 1 : 1 at long HNO_3 exposure. We emphasize that the present mass balance argument only addresses the average composition of the condensed phase at any one time, and that possible inhomogeneities in sample composition as probed by depth profiling are therefore not accessible.

Fig. 6 shows the phase diagram of the HNO_3–H_2O system obtained by Hanson and Mauersberger,[8] including the partial pressures of both HNO_3 and H_2O observed from our prolonged uptake experiments of HNO_3 on ice. Partial pressures were measured at the steady state after an abrupt change attributed to a phase transition such as displayed in Fig. 5. Experiments performed at 180 K reveal partial pressures corresponding to the co-existence curve between trihydrate and monohydrate, which is in good agreement with the results from mass balance experiments [$n = 3$, Fig. 5(a), $t = 640$ s]. At 190 and 200 K, the observed partial pressures clearly correspond to those of HNO_3 monohydrate or some undefined mixture for $n > 1$ [Fig. 5(b), $t = 550$ s]. However, it must be pointed out that the present experiments do not distinguish between crystalline and amorphous phases of the same stoichiometry. In order to describe the phases more precisely, spectroscopic studies of the condensed phase must be carried out as has recently been done by Tolbert and co-workers.[13,19]

3. HNO_3 diffusion in the ice. The prolonged uptake experiments allow us to determine the amount of HNO_3 which adsorb on the ice sample before the H_2O partial pressure monitored at m/z 18 begins to decrease in the reactor, for instance at $t \approx 250$ s and at the transition $t \approx 550$ s displayed in Fig. 5(b). The detailed results are given in the ESI,† where the amounts of absorbed HNO_3 are expressed in formal monolayers (ML) of HNO_3 assuming that one HNO_3 formal monolayer corresponds to 5×10^{14} molecules cm^{-2}. One observes for the first case that between 10 and 35 ML of HNO_3 have been adsorbed on the ice sample whereas at the transition point between 50 and 500 ML have been adsorbed.

The phase transition appears after a delay of the order of 200 s, during which the HNO_3 molecules can diffuse into the bulk of the ice. Fick's first law [eqn. (10)] describes a stationary process of molecular diffusion and was used to calculate the effective distance of penetration of HNO_3, d, into the bulk:

$$J = -D \frac{\partial C(x, t)}{\partial x} \tag{10}$$

where J is the flux of HNO_3, which may be expressed in our case by

$$J = \frac{F^{in} - F^{out}}{A_s} \tag{11}$$

where F^{in} and F^{out} are the HNO_3 flow entering and leaving the reactor, respectively, in molecules s^{-1}, D is the diffusion

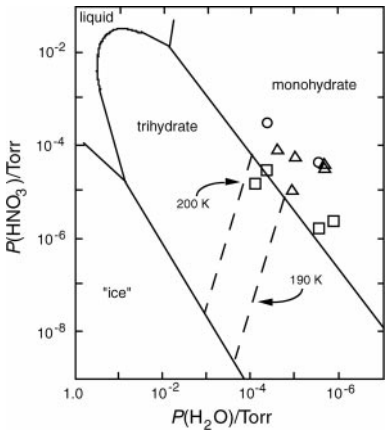

Fig. 6 HNO_3–H_2O phase diagram with partial pressures of HNO_3 plotted against pressure of H_2O observed during prolonged uptake experiments on HNO_3 on ice at (□) 180, (○) 190 and (△) 200 K. Solid lines are the co-existence curves and dashed lines are measured pressures over trihydrates observed by Hanson and Mauersberger[8] at a fixed temperature (NAT phase diagram from Hanson and Mauersberger[8]).

coefficient of HNO_3 in the ice and $\partial C/\partial x$ is the concentration gradient of HNO_3 in the condensed ice sample. This gradient may be approximated by a linear relationship using the known amount of HNO_3 taken up into the unknown volume $V = A_s d$. The gradient of HNO_3 in the ice substrate may therefore be expressed by the following expression:

$$\frac{\partial C(x, t)}{\partial x} \approx \frac{C(0, t) - C(h, t)}{d} = \frac{N(HNO_3)}{Vd} \quad (12)$$

where $N(HNO_3) = (F^{in} - F^{out})t$ is the number of HNO_3 molecules adsorbed on the ice sample during the time t. By substituting eqns. (11) and (12) into Fick's first law, eqn. (10), one obtains the following known equation for d, the diffusion length:

$$d = \sqrt{Dt} \quad (13)$$

Under the conditions that Fick's law is applicable to our experimental conditions, one obtains the well known relation for the diffusion length (see ESI†). At low temperatures (180, 190 K) one obtains a mean value of 15 ± 8 nm and at 200 K a mean diffusion length of 68 ± 22 nm is obtained at the phase transition with $D = 1.37 \times 10^{-2610/T}$ measured by Thibert and Dominé[26] for single crystal ice. If the condensed phase is amorphous, the diffusion lengths, d, are lower limits. At 180 K, the diffusion length represents 10% of the remaining ice thickness, whereas at 190 and 200 K the diffusion length is of the order of 100% of the remaining substrate on the support at phase transition. If we take a value 100 times larger for D, as has been reported repeatedly in the literature for amorphous or bulk ice substrates, the penetration depths d increase accordingly by a factor of 10. The message is that even at 180 K HNO_3 may have sufficient time to diffuse across the condensate in order to change the bulk composition.

B. HNO_3 on frozen H_2SO_4–H_2O

We performed SS uptake experiments of HNO_3 on solid frozen H_2SO_4–H_2O samples at different concentrations from 10 to 98% at two different temperatures, 180 and 200 K. Two types of SS experiments were performed, one with and one without external water flow, the primary purpose of which is to equilibrate the substrate interface. Fig. 7 shows typical SS experiments ($F^{in}_{HNO_3} \approx 10^{14}$ molecules s^{-1}) without external water flow performed at 180 K at three different H_2SO_4 concentrations, namely 17, 60 and 98 wt.%. One observes a constant HNO_3 rate of uptake at 17 and 60 wt.% H_2SO_4 solid samples, whereas partial saturation of the uptake rate is observed on 98 wt.% H_2SO_4 sample.

The initial uptake coefficients obtained on frozen H_2SO_4 solutions are displayed in Fig. 8, the uncertainties of which are of the order of 30%. These γ values have not been corrected according to eqn. (9). As discussed above regarding the interaction of HNO_3 on pure ice, the correction applied would be negligible at high HNO_3 flow rates, such as used in the interaction of HNO_3 on frozen H_2SO_4–H_2O. The top and bottom panels in Fig. 8 show the results measured at 180 and 200 K, respectively. At both temperatures one observes the same behavior. In experiments performed without external H_2O flow (open squares in Fig. 8), the uptake coefficient decreases with increasing H_2SO_4 concentration. The H_2O partial pressure inside the reactor gradually decreases during an uptake experiment without balancing H_2O flow. By pumping on the sample at a given concentration of H_2SO_4, the H_2SO_4 concentration at the surface may increase because of evaporation of H_2O and limiting condensed phase diffusion of H_2O. This may lead to a change in the concentration at the interface during an uptake experiment. One notes that even at the lowest H_2SO_4 concentration, γ is smaller than for both types of pure ice samples. The uptake coefficient decreases from 0.3 to 0.2 at 180 K and from 0.2 to 0.1 at 200 K on going from pure ice to a 10 wt.% H_2SO_4 solid solution. At 98 wt.% H_2SO_4, γ decreases to 0.05 and 0.03 at 180 K and 200 K, respectively. Fig. 8 shows that between these two limits of H_2SO_4 concentration, γ decreases linearly by a factor of 10 for experiments performed without external H_2O flow.

In the experiments performed with an external H_2O flow (closed diamonds in Fig. 8), one observes a constant uptake coefficient at H_2SO_4 concentrations $\leqslant 60$ wt.% of $\gamma = 0.21 \pm 0.005$ at 180 K and at H_2SO_4 concentrations $\leqslant 70$ wt.%, $\gamma = 0.10 \pm 0.02$ at 200 K, where the uncertainties correspond to one standard deviation. Beyond this threshold of 60 wt.% H_2SO_4, γ rapidly decreases to reach values of the order of 0.01. We also observe saturation of the uptake kinetics of HNO_3 on the H_2SO_4 frozen sample at these high H_2SO_4 concentrations such as displayed in Fig. 7. At 180 K the saturation of the uptake rate appears at 90 wt.% H_2SO_4, whereas at 200 K it occurs at 60 wt.% H_2SO_4. Therefore, Fig. 8 only displays the initial uptake coefficient γ_0 for these latter conditions. Generally, the steady-state uptake coefficient γ_{ss} is smaller by up to a factor of two compared with γ_0, as shown in Fig. 7.

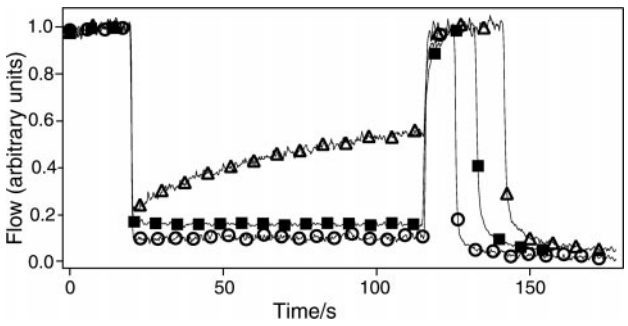

Fig. 7 Steady-state uptake experiments on HNO_3 at 180 K on H_2SO_4–H_2O frozen solutions without H_2O external flow at three different H_2SO_4 concentrations: (○) 17, (■) 60 and (△) 98 wt.%.

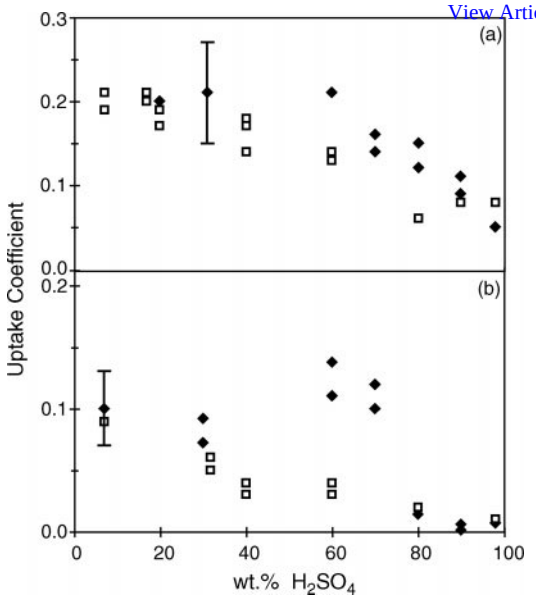

Fig. 8 Uptake coefficient γ of HNO_3 on H_2SO_4–H_2O frozen solutions as a function of H_2SO_4 concentration. Open squares represent uptake experiments performed without an external H_2O flow and full diamonds represent experiments with an additional H_2O flow to equilibrate the ice sample at (a) 180 and (b) 200 K. Statistical uncertainties were determined as $\pm 30\%$ for each individual measurement owing to signal noise and the uncertainty in the HNO_3 calibration.

Table 3 Uptake coefficients, γ, of HNO_3 on H_2SO_4–H_2O

T/K	γ	H_2SO_4 (wt.%)	Ref.
188	0.25 ± 0.05	15–87	Reihs *et al.*, 1990[28a]
191	$\geqslant 0.30$	57.7	Hanson, 1992[18b]
200	$\geqslant 0.20$	57.7	Hanson, 1992[18b]
223	0.07 ± 0.01	15–87	Reihs *et al.*, 1990[28a]
230	0.002	75	Tolbert *et al.*, 1988[27a]
283	0.11 ± 0.01	73	Van Doren *et al.*, 1991[29a]
180	0.207 ± 0.005	$\leqslant 60$	This work[b]
	$0.21 \rightarrow 0.05$[c]	>60	This work[b]
200	0.10 ± 0.02	$\leqslant 70$	This work[b]
	0.007 ± 0.005	>70	This work[b]

[a] Liquid solutions (or droplets). [b] Frozen crystalline solid. [c] See Fig. 8.

Table 3 summarizes the results of the present and previous work performed on liquid[27–29] and frozen H_2SO_4 solutions.[18] We observe the same trend in γ values as Reihs *et al.*[28] observed with liquid H_2SO_4. The mechanism proposed for the interaction of HNO_3 with H_2SO_4 at low temperature consists of both solvation and aqueous phase reaction of HNO_3. The lower γ obtained at higher H_2SO_4 concentration results from the solubility limitation of HNO_3 in H_2SO_4 on the sample surface.[28] The condensed phase products of the interaction of HNO_3 on solid H_2SO_4 substrates may be of two different compositions. One possibility is the formation of an HNO_3 hydrate on the H_2SO_4 surface. FTIR experiments performed by Iraci *et al.*[30] showed the growth of NAT in/on both liquid and crystalline H_2SO_4 films. The second possibility may be the formation of a saturated ternary solution when HNO_3 is added to H_2SO_4.

C. HNO_3 on solid ternary solutions

SS and PV experiments were performed on solid ternary solutions (STS) at different temperatures relevant to the lower stratosphere. Carslaw *et al.*[31] calculated the composition of H_2SO_4–HNO_3–H_2O aerosols resulting in PSC formation in the temperature range 185–200 K. We performed uptake experiments on STS using these calculated compositions. The solid samples were prepared in the same way as described earlier for H_2SO_4 samples and the ice surface was equilibrated by an external H_2O flow. When the plunger is lifted without an HNO_3 flow entering the reactor, one observes an HNO_3 partial pressure which has been taken into account in the calculation of γ. The γ values obtained on STS samples in the temperature range 185–195 K are constant and centered around a mean value of $\gamma = 0.10 \pm 0.03$ over the whole temperature range, thus for all compositions. At 200 K the STS composition is calculated to be 60 wt.% H_2SO_4 and 0.1 wt.% HNO_3. Owing to the small amount of HNO_3 in the STS composition at 200 K, the corresponding HNO_3 uptake coefficient has been assumed to be the same as that obtained for a binary frozen solution of 60 wt.% H_2SO_4, namely $\gamma = 0.1$ at 200 K (Fig. 8). No saturation of the rate of HNO_3 uptake on STS was observed for the concentration range studied. In relation to the interaction of HNO_3 on pure ice, the γ value for the interaction of HNO_3 on cold STS samples is lower by a factor of 2–3. The presence of HNO_3 (in excess of 1 wt.%) dissolved in H_2SO_4 decreases the rate of uptake of HNO_3 on low temperature samples compared with pure ice.

D. Modeling of experimental results for HNO_3 on ice

In order to understand the mechanism of the adsorption of HNO_3 on ice samples, we fitted our experimental results using a Langmuir–Hinshelwood model as described previously.[32] The proposed model consists of a set of two equations, representing a series of two elementary processes [eqns. (14) and (15)]:

$$G + ss \rightleftharpoons A \qquad k_1, k_{-1} \qquad (14)$$

$$A \rightleftharpoons B + ss \qquad k_2, k_{-2} \qquad (15)$$

Eqn. (14) considers that the gaseous HNO_3 (G) interacts with a free surface site ss located on the ice surface leading to a precursor species (A) in an effective bimolecular reaction. The rate of this reaction is therefore proportional to the number of free surface sites ss and to the HNO_3 concentration in the gas phase. The second step, eqn. (15), takes into account the liberation of a free ss by the formation of a new species (B). This step sets free surface sites which are again available to interact with G, thus avoiding any surface saturation, as was observed experimentally. Eqn. (15) may correspond to the diffusion process of adsorbed HNO_3, A, into deeper layers of the bulk.

We run the model according to two different procedures. First, one performs calculations using only eqn. (14) and the results are presented in Fig. 9(a1–3). Subsequently, both equations are used and the results are displayed in Fig. 9(b1–3). The running numbers 1–3 represent HNO_3 uptake experiments performed at three different HNO_3 flow rates entering the reactor at 200 K, namely a high (8×10^{15} molecules s^{-1}), a medium (1×10^{14} molecules s^{-1}) and a low (8×10^{12} molecules s^{-1}) HNO_3 flow rate, respectively. In the interest of simplification we did not consider the wall contribution of HNO_3 sticking on Teflon as has been discussed above. The results in Fig. 9 show a comparison between experimental MS signals (solid lines) and calculations (dotted lines) at 200 K.

The adjustable parameters in this model are the four kinetic constants (k_1, k_{-1} and k_2, k_{-2}) and the total number of surface sites ss (S_0). The best fits, presented in Fig. 9, were obtained using the set of kinetic parameters displayed in

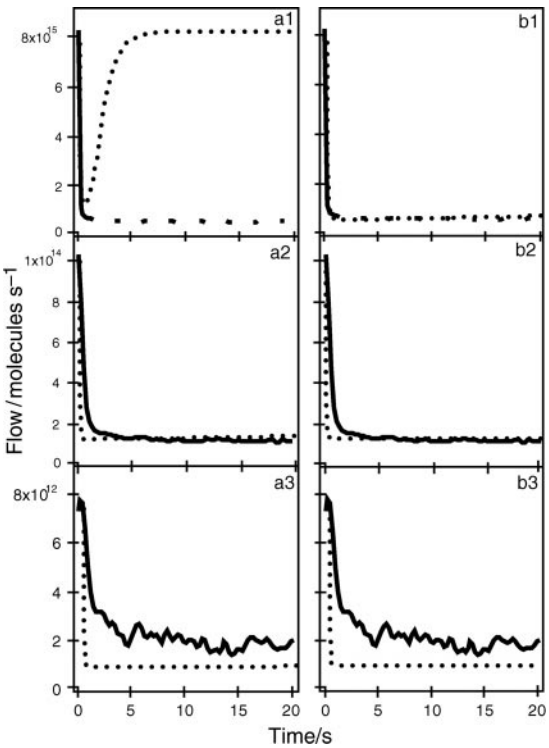

Fig. 9 Modeling of typical SS experiments. Comparison of experiments at 200 K (solid lines) and models (dotted lines). (a1–3) Simulation results for the adsorption of HNO_3 on ice samples at three different HNO_3 flow rates entering the reactor using the model described in eqn. (14). (b1–3) Simulation results of the same experimental data as in cases (a1–3) using the model described by eqn. (14) and (15).

Table 4 Set of parameters used in the modeling

Parameter	Units[a]	Numerical value[a]
S_0	**molecule**	**1.6×10^{16}**
	molecule cm^{-2}	9.4×10^{14}
k_1	**molecule^{-1} s^{-1}**	**8.7×10^{-16}**
	cm^2 molecule^{-1} s^{-1}	1.5×10^{-14}
k_{-1}	**s^{-1}**	**0.5×10^{-3}**
	cm^{-1} s^{-1}	4.6×10^{-6}
k_2	**s^{-1}**	**5.0**
	cm^{-1} s^{-1}	85.0
k_{-2}	**molecule^{-1} s^{-1}**	**0.1×10^{-16}**
	cm^2 molecule^{-1} s^{-1}	1.7×10^{-16}

[a] Bold characters represent the rate constants expressed for the present experimental system; the others are transferable units for unity surface-to-volume ratio. Rate constants in units of cm^{-1} s^{-1} are calculated using the value $A_s/V = 17/1830 = 9.3 \times 10^{-3}$ cm^{-1}.

Table 4. As described earlier,[32,33] the bold characters in Table 4 are values expressed for our specific experimental configuration whereas the other are expressed in transferable units independent of the experimental apparatus used.

The term $k_1 S_0$ corresponds to the rate of loss from the gas phase of the G species and is equal to 14 s^{-1}, which leads to a γ value of 0.19 according to eqn. (6) using a calculated collision frequency ω of 74 s^{-1}. This is the experimental mean value of γ for the interaction of HNO_3 with pure ice at 200 K obtained in this study. In Fig. 9(b1–3), one notes the excellent agreement between the calculated curves (dotted lines) and the experimental results (solid lines). The calculated rate of HNO_3 uptake displayed in Fig. 9(a1) shows that using a high HNO_3 flow rate, one rapidly reaches the initial level due to rapid saturation of the free surface site ss. No saturation is observed when a precursor species is introduced in the adsorption mechanism as displayed in Fig. 9(b1): the calculated rate of uptake fits the experimental result fairly well. Using a medium HNO_3 flow rate, both calculated and experimental uptake curves are the same in both runs [cases (a2) and (b2)]. Calculations overestimate uptake experiments performed using a low HNO_3 flow rate as displayed in Fig. 9(b3). This stems from the fact that we did not consider the amount of HNO_3 desorbing from the reactor wall. In this last case, the wall effect contributes an additional HNO_3 flow of 1×10^{12} molecules s^{-1}, which is the difference between the experimental and calculated flow rates. This confirms that at low HNO_3 flow rates the correction to the kinetics is more important than at high flow rates, where the HNO_3 wall contribution is negligible.

Conclusions and atmospheric implications

We measured the uptake of HNO_3 on both vapor-condensed (C) and bulk (B) ice in the temperature range 180–211 K. The Arrhenius representation shows two distinct regimes of temperature dependence. At low temperatures ($T < 195$ K), the kinetics of adsorption are constant and relatively high ($\gamma \approx 0.3$). At higher temperatures, we determined an activation energy $E_a = -7 \pm 1$ kcal mol^{-1}. For a specific temperature, γ is independent of the HNO_3 flow entering the reactor, which allows us to conclude that the rate law is first order in [HNO_3]. At $T \leqslant 210$ K no saturation of the rate of uptake on ice was observed, leading to $\gamma_0 = \gamma_{ss}$. Considering a PSC type II surface area of 10^{-7} cm^2 cm^{-3},[34] and $\gamma = 0.26$ for HNO_3 adsorption on pure ice at 187 K such as measured in this study, one obtains a lifetime of 1.7 h for HNO_3. Uptake of HNO_3 on PSC type I clouds, whose surface area is 10 times smaller than for type II, the HNO_3 lifetime would be approximately 1.5 days using an uptake coefficient of the order of 0.1.

Long exposure of the ice sample to gaseous HNO_3 allows one to observe a phase transition during the uptake of nitric acid. At this phase transition between 50 and 500 formal HNO_3 monolayers were adsorbed on the ice sample, diffusing into a surface layer of 15 nm (180, 190 K) and 70 nm (200 K) thick provided that the condensed phase is crystalline ice. These experiments led us to a mean stoichiometric ratio of the condensate of $HNO_3 \cdot 3H_2O$ at 180 K and $HNO_3 \cdot nH_2O$ with $0.9 \leqslant n \leqslant 1.8$ at 190 and 200 K. These experiments did not allow us to confirm unambiguously the formation of NAM (nitric acid monohydrate) and NAT at the interface at 180 K and 190 or 200 K, respectively. The values of the mean ratio obtained in this study at 180 K are in good agreement with the expected calculated composition of type Ia STS aerosols at 188 K.[13,31,35]

As first suggested by Wofsy *et al.*,[36] HNO_3 is thought to reduce H_2O evaporation rate from ice particles, which has been confirmed by others[16,19,37,38] claiming that one HNO_3 monolayer decreases the H_2O partial pressure to a significant, and therefore measurable, extent. In this study we found that many more than one HNO_3 monolayer is indeed needed to reduce the H_2O evaporation rate. We therefore confirm that the adsorption of HNO_3 influences the evaporation rate of water, in contrast to the results obtained by Biermann *et al.*[39] This result suggests that for small ice particles HNO_3 may be distributed across the entire bulk at 190 and 200 K. Even at temperature as low as 180 K, the penetration depth of HNO_3 in the bulk may be significant.

Kinetic results of the interaction of HNO_3 on frozen H_2SO_4 samples show an abrupt change at 60 wt.% H_2SO_4 at 180 and 200 K. At concentrations lower than this threshold the uptake coefficient is constant, albeit smaller that on pure ice. Above this concentration the γ values decrease significantly to reach 0.03.

When HNO_3 is added to H_2SO_4 to form solid ternary solutions, the kinetics of the interaction are significantly slower with respect to pure ice and binary solutions at H_2SO_4 concentrations below 60 wt.%. We observed a constant value of $\gamma = 0.1$ on all STS compositions studied in this work in the temperature range 185–195 K.

Owing to the fast uptake kinetics of HNO_3 on the low temperature surfaces studied in this work, nitric acid is continuously removed by sedimentation, ultimately leading to denitrification. This results in lower concentrations of available NO_x in the upper troposphere and the lower stratosphere.[36] This denitrification is occasionally observed,[40,41] and this low level of NO_x may contribute to an increase in ozone depletion, because the catalytic cycle of ozone destruction cannot be halted by the conversion of the unstable ClO to stable $ClONO_2$.

Acknowledgements

Funding for this work was provided by the Office Fédéral de l'Enseignement et de la Science (OFES) in the framework of the subprojects COBRA and CUTICE of the EU program "Environment and Climate". We thank Professor Hubert van den Bergh for his lively interest and input.

References

1 A. Laaksonen, J. Hienola, M. Kulmala and F. Arnold, *Geophys. Res. Lett.*, 1997, **24**, 3009.
2 J. Lelieveld, B. Bregman, F. Arnold, V. Bürger, P. J. Crutzen, H. Fischer, A. Waibel, P. Siegmund and P. F. J. van Velthoven, *Geophys. Res. Lett.*, 1997, **24**, 603.
3 H. B. Singh, Y. Chen, G. L. Gregory, G. W. Sachse, R. Talbot, D. R. Blake, Y. Kondo, J. D. Bradshaw, B. Heikes and D. Thornton, *Geophys. Res. Lett.*, 1997, **24**, 127.
4 P. J. LeBel, B. J. Huebert, H. I. Schiff, S. A. Vay, S. E. Vanbramer and D. R. Hastie, *J. Geophys. Res.*, 1990, **95**, 10199.
5 W. F. J. Evans, C. T. McElroy and I. E. Galbally, *Geophys. Res. Lett.*, 1985, **12**, 825.
6 D. R. Hanson, *Geophys. Res. Lett.*, 1997, **24**, 1087.

7 H. S. Johnston, S. Chang and G. Whitten, *J. Phys. Chem.*, 1974, **78**, 1.
8 D. R. Hanson and K. Mauersberger, *Geophys. Res. Lett.*, 1988, **15**, 855.
9 D. R. Hanson, A. R. Ravishankara and E. R. Lovejoy, *J. Geophys. Res.*, 1996, **101**, 9063.
10 D. R. Hanson, *J. Phys. Chem.*, 1998, **102**, 4794.
11 A. Allanic, R. Oppliger and M. J. Rossi, *J. Geophys. Res.*, 1997, **102**, 23529.
12 R. Oppliger, A. Allanic and M. J. Rossi, *J. Phys. Chem.*, 1997, **101**, 1903.
13 M. A. Zondlo, S. B. Barone and M. A. Tolbert, *J. Phys. Chem.*, 1998, **102**, 5735.
14 J. P. D. Abbatt and M. J. Molina, *Geophys. Res. Lett.*, 1992, **19**, 461.
15 D. R. Hanson and A. R. Ravishankara, *Geophys. Res. Lett.*, 1995, **22**, 385.
16 T. Peter, R. Müller, P. J. Crutzen and T. Deshler, *Geophys. Res. Lett.*, 1994, **21**, 1331.
17 M. A. Tolbert and A. M. Middlebrook, *J. Geophys. Res.*, 1990, **95**, 22423.
18 D. R. Hanson, *Geophys. Res. Lett.*, 1992, **20**, 2063.
19 M. A. Zondlo, S. B. Barone and M. A. Tolbert, *Geophys. Res. Lett.*, 1997, **24**, 1391.
20 F. Caloz, F. F. Fenter, K. Tabor and M. J. Rossi, *Rev. Sci. Instrum.*, 1997, **68**, 3172.
21 F. F. Fenter, F. Caloz and M. J. Rossi, *J. Phys. Chem.*, 1994, **98**, 9801.
22 L. Chaix, H. van den Bergh and M. J. Rossi, *J. Phys. Chem.*, 1998, **102**, 10300.
23 M. T. Leu, *Geophys. Res. Lett.*, 1988, **15**, 17.
24 J. P. D. Abbatt, *Geophys. Res. Lett.*, 1997, **24**, 1479.
25 S. Seisel, B. Flückiger and M. J. Rossi, *Ber. Bunsen-Ges. Phys. Chem.*, 1998, **102**, 811.
26 E. Thibert and F. Dominé, *J. Phys. Chem.*, 1998, **102**, 4432.
27 M. A. Tolbert, M. J. Rossi and D. A. Golden, *Geophys. Res. Lett.*, 1988, **15**, 847.
28 C. M. Reihs, D. M. Golden and M. A. Tolbert, *J. Geophys. Res.*, 1990, **95**, 16545.
29 J. M. Van Doren, L. R. Watson, P. Davidovits, D. R. Worsnop, M. S. Zahniser and C. E. Kolb, *J. Phys. Chem.*, 1991, **95**, 1684.
30 L. T. Iraci, A. M. Middlebrook, M. A. Wilson and M. A. Tolbert, *Geophys. Res. Lett.*, 1994, **21**, 867.
31 K. S. Carslaw, B. P. Luo, S. L. Clegg, P. Brimblecombe and P. J. Crutzen, *Geophys. Res. Lett.*, 1994, **21**, 2479.
32 A. Aguzzi and M. J. Rossi, *Phys. Chem. Chem. Phys.*, 1999, **1**, 4337.
33 K. Tabor, L. Gutzwiller and M. J. Rossi, *J. Phys. Chem.*, 1994, **98**, 6172.
34 R. Turco, O. B. Toon and P. Hamill, *J. Geophys. Res.*, 1989, **94**, 16493.
35 A. Tabazadeh, R. P. Turco, P. Drdla, M. Z. Jacobson and O. B. Toon, *Geophys. Res. Lett.*, 1994, **21**, 1619.
36 S. C. Wofsy, R. J. Salawitch, J. H. Yatteau, M. B. McElroy, B. W. Gandrud, J. E. Dye and D. Baumgardner, *Geophys. Res. Lett.*, 1990, **17**, 449.
37 F. E. Livingston and S. M. George, *J. Phys. Chem. A*, 1998, **102**, 10280.
38 M. S. Warshawsky, M. A. Zondlo and M. A. Tolbert, *Geophys. Res. Lett.*, 1999, **26**, 823.
39 U. M. Biermann, J. N. Crowley, T. Huthwelker, G. K. Moortgat, P. J. Crutzen and T. Peter, *Geophys. Res. Lett.*, 1998, **25**, 3939.
40 Y. Kondo, H. Irie, M. Koike and G. E. Bodeker, *Geophys. Res. Lett.*, 2000, **27**, 337.
41 A. E. Dessler, J. Wu, M. L. Santee and M. R. Schoeberl, *J. Geophys. Res.*, 1999, **104**, 13993.